

Interparticle Charge Transfer Mediated by π - π Stacking of Aromatic Moieties

Sulolit Pradhan, Debraj Ghosh, Li-Ping Xu, and Shaowei Chen*

Department of Chemistry and Biochemistry, University of California, Santa Cruz, California 95064

Received April 13, 2007; E-mail: schen@chemistry.ucsc.edu

Lately intense research interests have been focused on the electronic conductivity properties of transition-metal nanoparticles (e.g., Au, Pd, and Ag) that are passivated by an organic monolayer (i.e., the so-called monolayer-protected nanoparticles).¹ With such a core-shell composite nanostructure, the resulting conductivity can be tailored by the combined effects of the conductive inorganic cores and the insulating organic shells, where the cores dictate the Coulomb blockade characteristics while the organic shells serve as the insulating barrier of interparticle charge transfer.² In addition, the collective conductivity properties of their organized assemblies are found to be determined not only by the particle chemical structure (core size, shape, and surface ligands) but also by the specific chemical environments and interparticle interactions as well.²

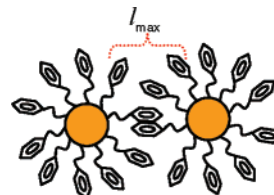
Toward this end, electrochemistry has been a powerful tool in the evaluation of the electronic conductivity of nanoparticle solids. In particular, in conjunction with the Langmuir and Langmuir-Blodgett (LB) techniques, one can readily manipulate the interparticle separation and concurrently examine the particle ensemble conductance, leading to the establishment of an unambiguous correlation between the particle ensemble structure and conductivity properties, in contrast to dropcast thick films.³⁻⁵

For instance, Heath and co-workers⁶ studied the electrical characteristics of a Langmuir monolayer of alkanethiolate-protected silver (AgSR) nanoparticles at the air-water interface by examining the corresponding linear and nonlinear ($\chi^{(2)}$) optical responses and observed a transition from insulator to metal when the interparticle spacing was sufficiently small. Such a transition was also manifested in electrochemical impedance measurements.⁶ Using scanning electrochemical microscopy (SECM), Bard et al.⁷ also observed a similar metal-insulator transition of AgSR nanoparticle monolayers at the air-water interface by monitoring the feedback currents at varied surface pressures (and interparticle separations). More recently, we observed that by deliberate control of the nanoparticle structures and interparticle interactions, single electron-transfer could also be achieved in LB thin films of monodisperse gold nanoparticles.⁸

Yet, these earlier studies are mostly focused on nanoparticles passivated by an alkanethiolate monolayer; and effects of aromatic functional groups on the interparticle charge transfer have remained largely unexplored. Murray and co-workers³ examined the conductivity properties of dropcast thick films of a series of gold nanoparticles with varied arenethiolate protecting shells and observed that the tunneling barriers of interparticle charge-transfer predominantly arose from the saturated segment of the organic capping ligands.

In this report, we investigated the electronic conductivity of LB monolayers of phenylethylthiolate-passivated gold (PET-Au) nanoparticles that were prepared at varied surface pressures (interparticle separations) and observed that the π - π stacking of the phenyl moieties from neighboring particles, which was manipulated by the Langmuir technique, played a critical role in the regulation of interparticle charge transfer. At interparticle separation

Scheme 1



where the phenyl moieties from adjacent particles were fully stacked, the interparticle conductance reached the maximum (Scheme 1). This may be exploited as a sensitive mechanism to mediate interparticle charge transfer.

The PET-Au particles were synthesized by adopting a literature synthetic protocol,⁹ with core diameters varied at 1.39 ± 0.73 nm (PET-I), 1.64 ± 0.79 nm (PET-II), and 2.97 ± 0.62 nm (PET-III), as determined by transmission electron microscopic measurements (Figure S1, Supporting Information). The monolayer films of these nanoparticles were first prepared by spreading a calculated amount of the particle solutions in toluene onto the water surface of an LB trough (NIMA 611D, a representative Langmuir isotherm was included as Figure S3) and then deposited onto an interdigitated arrays electrode (IDA, consisting of 25 pairs of gold fingers, $5 \mu\text{m} \times 5 \mu\text{m} \times 3$ mm, from ABTECH) by the LB method at varied interparticle separations. Structural integrity of the nanoparticle monolayers was examined by TEM and STM measurements where the interparticle separations were found to be in good agreement with the estimations based on the Langmuir isotherm (Tables S1 and S2). Electrochemical measurements were then carried out with an EG&G PARC 283 potentiostat/galvanostat in vacuo with a cryostat from Janis Research and at different temperatures (Lake-shore 331 temperature controller).

Insets of Figure 1 show some representative current-potential (I - V) profiles of the LB monolayers of the three nanoparticles synthesized above within the temperature range of 100 to 320 K. It can be seen that the I - V responses all exhibit linear (ohmic) behaviors, indicative of relatively strong interparticle electronic coupling, most probably as a result of the short ligand chains and aromatic moieties that facilitate interparticle charge transfer.³ In addition, the ensemble conductivity, as evaluated from the slope of the I - V profiles, increases with increasing particle core size, which can be accounted for by the enhanced interparticle dipolar interactions.^{10,11} The conductivity is also found to increase with increasing temperature, consistent with the semiconductor characteristics of the nanoparticles which are essentially nanoscale organic-inorganic composite materials. Also the temperature dependence of the ensemble conductivity exhibits a clear Arrhenius behavior at temperatures greater than or equal to 280 K (Figure S6), suggestive of a thermal activation mechanism for the interparticle charge-transfer driven by electron hopping.³

More interestingly, the ensemble conductivity (Figure 1) exhibits a volcano-shaped dependence on the interparticle separation for all three particles within the entire temperature range. This deviates drastically from our previous study¹² of Langmuir monolayers of

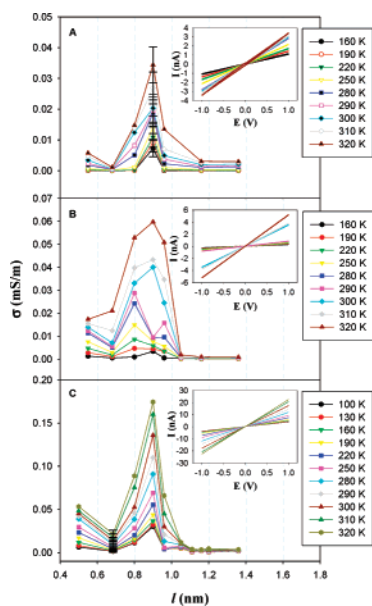


Figure 1. Variation of nanoparticle monolayer conductivity (σ) with interparticle edge-to-edge separation (l) at different temperatures for three PET–Au particles: (A) PET-I, (B) PET-II, and (C) PET-III. Error bars reflect statistical average of at least three measurements. Insets show the representative I – V profiles of the corresponding nanoparticles at $l = 0.90$ nm. Potential scan rate, 20 mV/s.

gold nanoparticle passivated by saturated alkanethiolates where the particle conductivity was found to exhibit an exponential decay with increasing interparticle separation. From Figure 1, one can see that the maximum conductivity corresponds to a narrow range of interparticle edge-to-edge distances (l) of ca. 0.8–1.0 nm. Note that in nanoparticle solids, ligand intercalation and hence the van der Waals (vdW) interactions between the ligands of adjacent particles play an important role in the determination of the energetic barrier for interparticle electron hopping. That is, the interparticle charge-transfer most probably consists of both through-bond and through-space (by way of the vdW contacts between interdigitated ligands) contributions. Thus, it can be envisioned that in the present study, the ligand vdW interactions will be enhanced by the π – π stacking of the phenyl moieties from adjacent particles. In fact, on the basis of Hyperchem calculations of the fully extended ligand chains, the interparticle edge-to-edge separation is anticipated to be ca. 1.11 nm when the phenyl rings are fully overlapped (Scheme 1; note that the phenyl ring is 0.28 nm in diameter and the optimal range of l is 0.8–1.0 nm, Figure 1). This is somewhat longer than the interparticle separation observed in Figure 1 for maximum ensemble conductance ($l_{\max} = 0.9$ nm for all three PET–Au particles within the entire temperature range under study). This may be, at least in part, ascribed to the tilting conformation of the ligands adsorbed onto the gold core surface. Furthermore, in reality the stacking of the phenyl moieties from neighboring particles may deviate somewhat from the ideal parallel configuration.

The mediation of interparticle charge transfer by π – π stacking of the aromatic moieties may also account for the substantially larger conductivity observed at l_{\max} with the nanoparticle monolayers than with their respective dropcast thick films (Figures S8), although the overall I – V responses are very similar (Figure S7). In dropcast films of alkanethiolate-protected nanoparticles, it is generally believed that the capping ligands between neighboring particles are fully intercalated.^{4,5} Yet, for arenethiolate-protected gold nanoparticles, Murray et al.³ proposed a model based on ligand head-to-head contacts to account for the solid-state electronic conductivity. For the PET–Au particles, this corresponds to $l = 1.36$ nm. From

Figure 1, it can be seen that this interparticle distance lies beyond the optimal range for maximum ensemble conductivity.

When compared to the monolayer conductivity at similar interparticle separation ($l = 1.36$ nm), the dropcast films (Figure S8) exhibit interesting variation of the conductivity with particle core size. For the smallest PET-I particles, the dropcast films exhibit a conductivity about 2 orders of magnitude smaller than the LB monolayers; for the larger PET-II particles, the monolayer conductivity becomes only several folds larger than that of the dropcast films; whereas for the largest PET-III particles, it is the opposite, the dropcast films now show a conductivity a few times that of the LB monolayers. This suggests that for smaller particles, the particle arrangements within the multilayer ensembles play a predominant role in the determination of the overall conductivity, whereas for larger particles, the enhanced contributions from interparticle dipolar (electronic) interactions become increasingly appreciable.^{10,11}

Furthermore, from the temperature dependence of the ensemble conductivity (Figure S8), one can see that the smaller the particle core size is, the steeper is the change of the conductivity with increasing temperature. Recently Murray et al.¹³ showed that thermally induced core motion led to drastic enhancement of the electronic conductivity of nanoparticle solids. It is anticipated that the core thermal motion will be stronger for smaller particles, consistent with the above experimental observations (Figure S8).

It has been recognized that the particle ensemble conductivity is the combined consequence of the interplay of at least three effects:² (i) the disorder due to the dispersity of particle core size, shape and chemical environments, (ii) the dipole coupling between adjacent particles, and (iii) the Coulomb repulsion of electrons (of opposite spins) on a given particle. The present study strongly suggests that the interparticle charge transfer can also be sensitively mediated by the vdW interactions between the functional moieties of the organic capping ligands from adjacent particles. Note that electron transport along a carbon nanotube telescope has also been found to exhibit an oscillation with the displacement of the outer tube relative to the inner tube, which is attributable to the periodic interwall π – π coupling.¹⁴ Such a controlling mechanism may be exploited for nanoscale sensing and switching applications.

Acknowledgment. This work was supported in part by the NSF (Grants CHE-0456130 and 0718170), and ACS–PRF (Grant 39729-AC5M).

Supporting Information Available: Additional experimental details and data analyses (Figures S1 to S8). This material is available free of charge via the Internet at <http://pubs.acs.org>.

References

- (1) Brust, M.; Walker, M.; Bethell, D.; Schiffrin, D. J.; Whyman, R. *J. Chem. Soc., Chem. Commun.* **1994**, 801.
- (2) Remacle, F.; Levine, R. D. *Chemphyschem* **2001**, *2*, 20.
- (3) Wuelfing, W. P.; Murray, R. W. *J. Phys. Chem. B* **2002**, *106*, 3139.
- (4) Wang, L. Y.; Shi, X. J.; Kariuki, N. N.; Schadt, M.; Wang, G. R.; Rendeng, Q.; Choi, J.; Luo, J.; Lu, S.; Zhong, C. J. *J. Am. Chem. Soc.* **2007**, *129*, 2161.
- (5) Ibanez, F. J.; Gowrishetty, U.; Crain, M. M.; Walsh, K. M.; Zamborini, F. P. *Anal. Chem.* **2006**, *78*, 753.
- (6) Collier, C. P.; Vossmeier, T.; Heath, J. R. *Annu. Rev. Phys. Chem.* **1998**, *49*, 371.
- (7) Quinn, B. M.; Prieto, I.; Haram, S. K.; Bard, A. J. *J. Phys. Chem. B* **2001**, *105*, 7474.
- (8) Pradhan, S.; Sun, J.; Deng, F.; Chen, S. W. *Adv. Mater.* **2006**, *18*, 3279.
- (9) Donkers, R. L.; Lee, D.; Murray, R. W. *Langmuir* **2004**, *20*, 1945.
- (10) Remacle, F.; Levine, R. D. *Isr. J. Chem.* **2002**, *42*, 269.
- (11) Snow, A. W.; Wohltjen, H. *Chem. Mater.* **1998**, *10*, 947.
- (12) Chen, S. W. *Anal. Chim. Acta* **2003**, *496*, 29.
- (13) Choi, J. P.; Coble, M. M.; Branham, M. R.; DeSimone, J. M.; Murray, R. W. *J. Phys. Chem. C* **2007**, *111*, 3778.
- (14) Grace, I. M.; Bailey, S. W.; Lambert, C. J. *Phys. Rev. B* **2004**, *70*, 153405.

JA072597P

Supporting Information

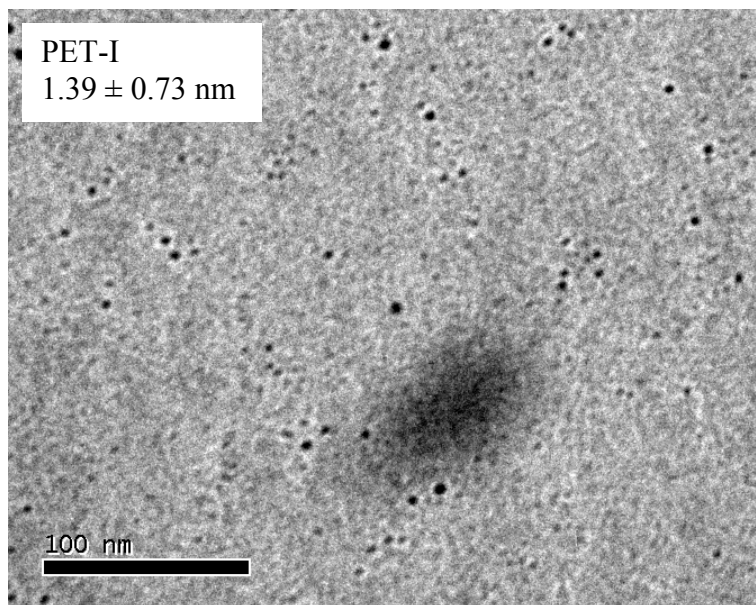
Interparticle Charge Transfer Mediated by π - π Stacking of Aromatic Moieties

Sulolit Pradhan, Debraj Ghosh, Li-Ping Xu, and Shaowei Chen*

*Department of Chemistry and Biochemistry, University of California, Santa Cruz,
California 95064*

Calculation of Nanoparticle Conductivity. From the I-V slopes, the film resistance (R) was calculated. Then by $49R = \rho(L/S)$, ρ and hence σ was estimated. Here L is the IDA electrode interfinger gap, 5 μm ; and S is the film cross section area approximated by (particle physical diameter, core + two ligands) \times (IDA finger length, 3 mm). The constant (49) reflects that there are totally 49 junctions which are in parallel within the IDA chip.

Transmission Electron Microscopy (TEM). The particle core diameter was measured with a JEOL 1200 EX Transmission electron microscope (TEM) operated at 80 keV. The samples were prepared by casting a drop of the particle solution in dichloromethane onto a 200-mesh carbon-coated copper grid. Particle core size was analyzed by using ImageJ software of the obtained micrographs including at least several hundred data points. The average particle core diameters are indicated in the respective figure legend below.



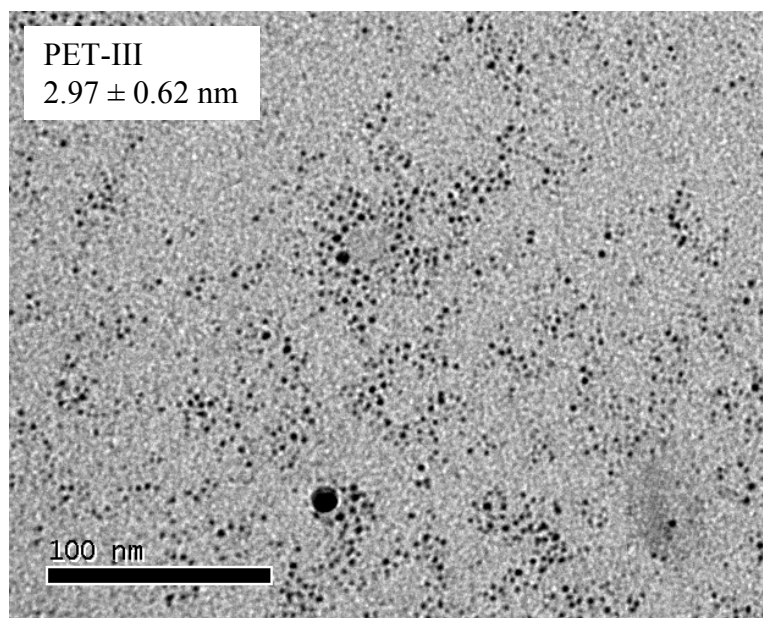
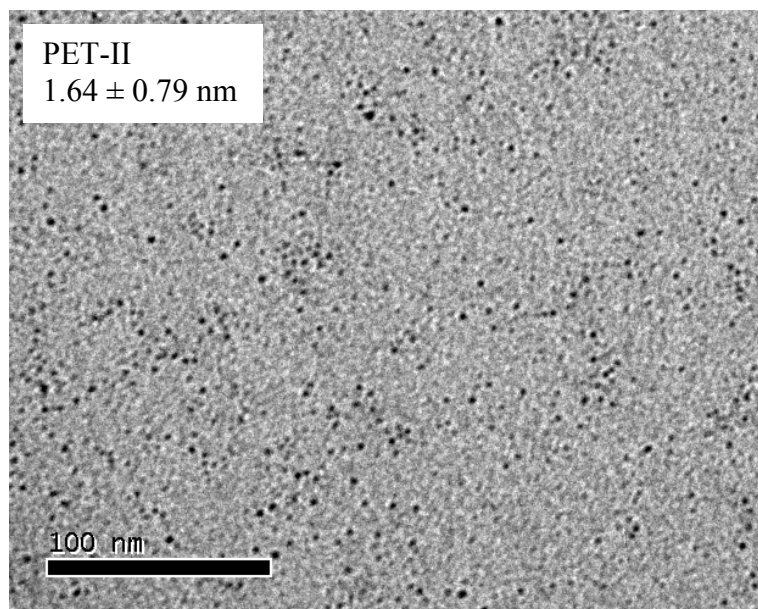


Figure S1. Representative TEM micrographs of PET-Au nanoparticles. Scale bars are all 100 nm.

Spectroscopy. The particle purity was examined by using ^1H NMR spectroscopy (Varian Unity 500 MHz) with a concentrated solution of particles dissolved in CDCl_3 . The absence of any sharp features suggests removal of excessive ligands from the particle samples. UV-visible spectroscopic measurements were carried out with a UNICAM ATI UV4 spectrometer. The typical concentration of the particle solution was $0.27\ \mu\text{M}$. The spectra are shown in Figure S2. It can be seen that the intensity of the surface plasmon resonance peak (ca. 520 nm) decreases in the order of PET-III > PET-II > PET-I, consistent with their core size estimations based on TEM data (Figure S1).

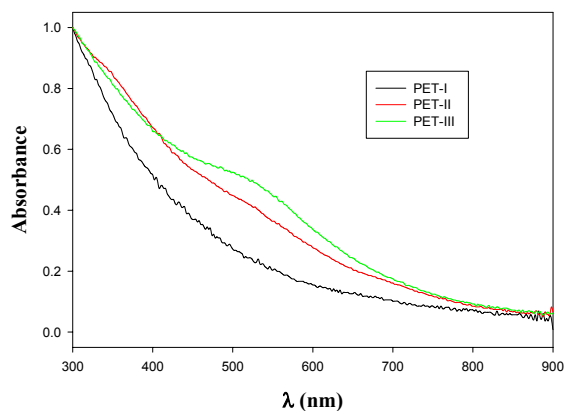


Figure S2. UV-Vis spectra of the three PET-Au nanoparticles. Particle concentration 1 mg/mL in toluene. Spectra were normalized to their respective absorbance at 300 nm.

Langmuir-Blodgett Monolayers of Nanoparticles. The monolayer films of the nanoparticles were prepared by spreading a calculated amount of the particle solutions in toluene onto the water surface of an LB trough (NIMA 611D) by using a Hamilton microliter syringe, and then deposited onto an interdigitated arrays electrode (IDA, consisting of 25 pairs of gold fingers, $5\ \mu\text{m} \times 5\ \mu\text{m} \times 3\ \text{mm}$, from ABTECH) by the LB method at varied interparticle separations. The dipper speed was controlled at 1 mm/min.

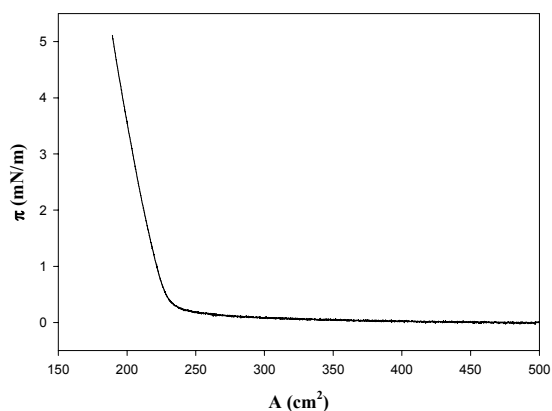
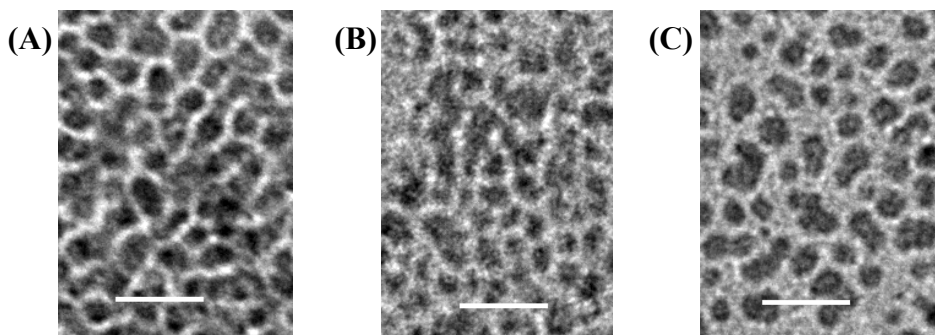


Figure S3. Representative Langmuir isotherm of PET-Au nanoparticles (PET-III). Particle concentration 1 mg/mL in toluene; amount spread 200 μL . Compression speed 10 cm^2/min .

Table S1 Selected comparison of the interparticle distances (I) calculated from the Langmuir isotherm and from TEM measurements for the PET-III nanoparticle monolayers

Langmuir Distance (nm)	TEM Distance (nm)	TEM Image (scale bar = 8.46 nm)
0.68	0.69 ± 0.12	(A)
0.80	0.77 ± 0.15	(B)
0.90	0.86 ± 0.22	(C)



Scanning Tunneling Microscopy (STM). To verify the structural integrity of the nanoparticle LB monolayer films, nanoparticle monolayers were also deposited onto a Au(111) substrate surface for STM studies (PicoLE SPM from Molecular Imaging) under exactly the same conditions as those for IDA deposition. In STM measurements, atomically flat Au(111) substrate was used which was coated a prior with a decanethiol self-assembled monolayer to render the surface hydrophobic and enhance the interactions with the particles. A mechanically cut Pt/Ir tip was used in the STM measurements.

Figure S4 depicts the STM images of four PET-III nanoparticle monolayers at varied interparticle separations. The insets show the histograms of the edge-edge distance as estimated from the corresponding STM topographs. Table S1 compares the distances from the STM measurements with those based on the deposition areas (Langmuir isotherm). It can be seen that they show very good agreement, though some deviation can be found at very large or very small interparticle separation.

Figure S5 shows similar measurements with the PET-I and PET-II nanoparticle monolayers. Both were deposited at $l = 0.90$ nm (from Langmuir isotherms). The distance as estimated from the STM measurement is somewhat larger, at 1.02 and 0.97 nm respectively.

Table S2 Interparticle distances (l) calculated from the Langmuir isotherm and from STM measurements for the PET-III nanoparticle monolayers

Langmuir Distance (nm)	STM Distance (nm)
0.69	0.58 ± 0.03
0.90	0.96 ± 0.07
1.11	1.12 ± 0.23
1.20	1.84 ± 0.18

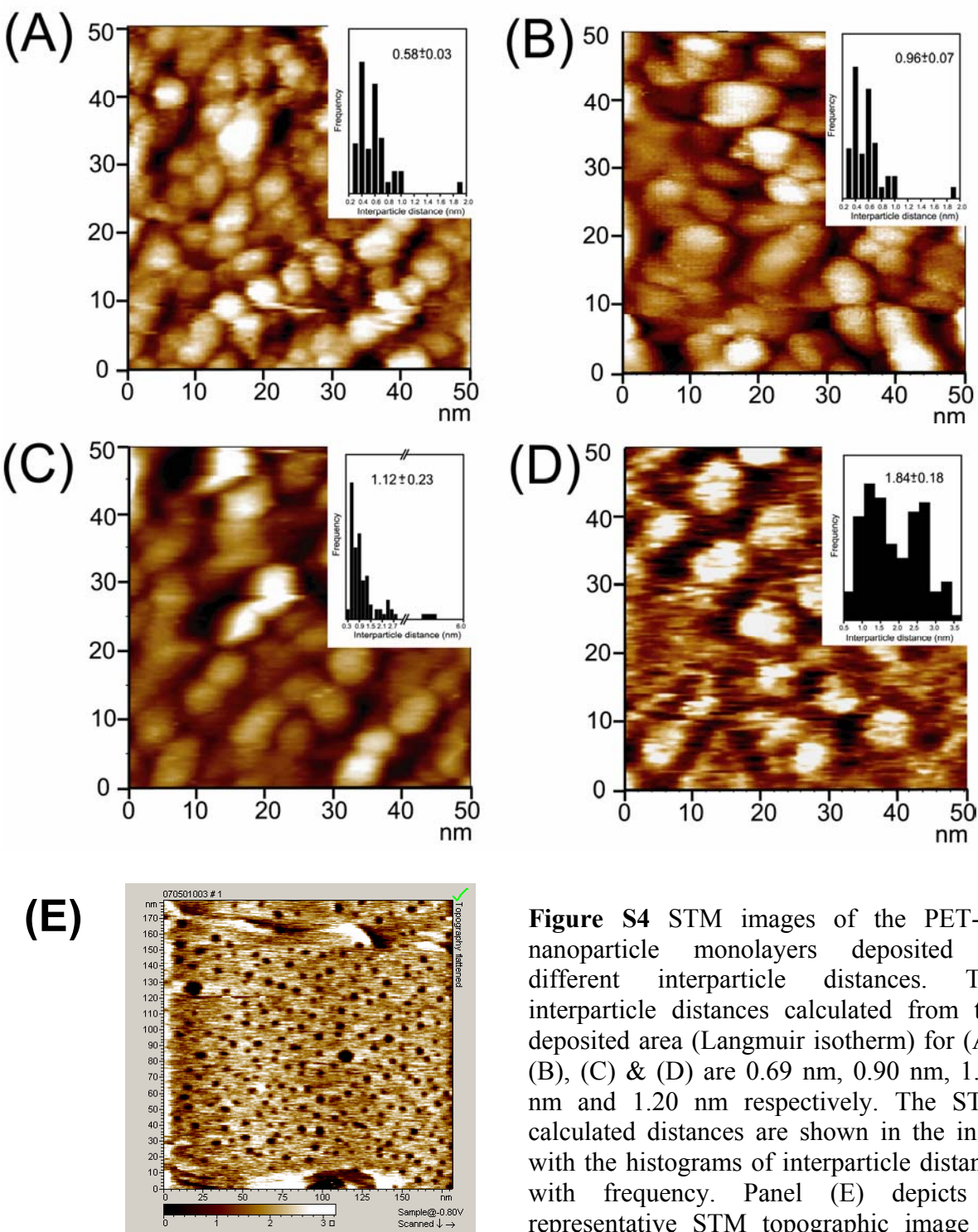


Figure S4 STM images of the PET-III nanoparticle monolayers deposited at different interparticle distances. The interparticle distances calculated from the deposited area (Langmuir isotherm) for (A), (B), (C) & (D) are 0.69 nm, 0.90 nm, 1.11 nm and 1.20 nm respectively. The STM calculated distances are shown in the inset with the histograms of interparticle distance with frequency. Panel (E) depicts a representative STM topographic image of the Au(111) coated with a decanethiol self-assembled monolayer prior to particle deposition.

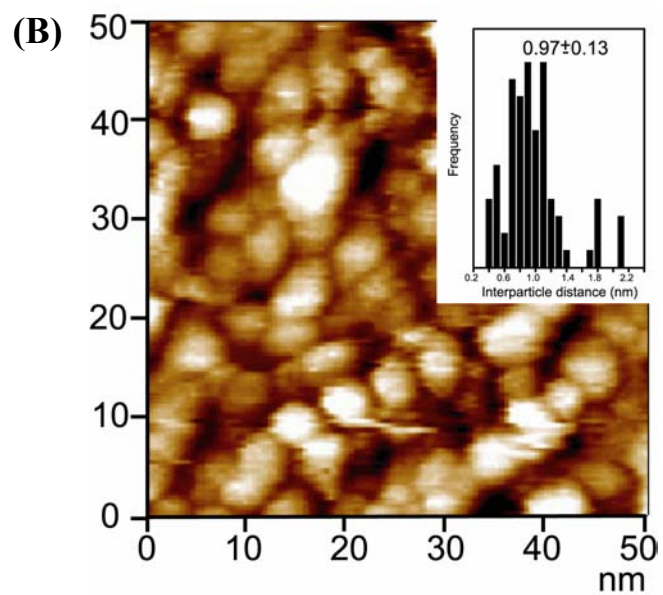
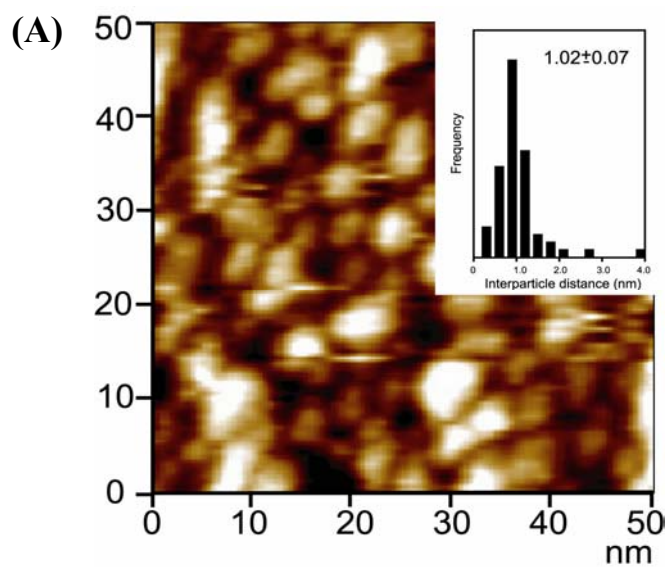
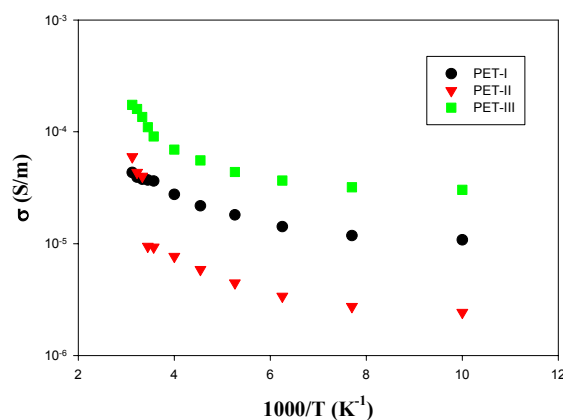


Figure S5 STM images of PET-I (A) and PET-II (B) nanoparticle monolayers at an interparticle distance of 0.90 nm as estimated from Langmuir isotherm based on the deposition area. The STM calculated distances are shown in the inset with the histograms of interparticle distance with frequency.

Electrochemistry. Electrochemical measurements were carried out with an EG&G PARC 283 Potentiostat/Galvanostat in vacuo with a cryostat from Janis Research and at different temperatures (Lakeshore 331 Temperature Controller).

Figure S6 shows a representative plot of the monolayer conductivity as a function of temperature. It can be seen that (i) the conductivity of the particle monolayers increases with increasing temperature; and (ii) at temperature ≥ 280 K, the particle conductivity exhibits a linear increase with T^{-1} with an activation energy much larger than that found at lower temperature (assuming similar Arrhenius behaviors). Such dual dependence of conductivity on temperature has also been observed previously with LB monolayers of alkanethiolate-protected nanoparticles and ascribed to the variation of interparticle charge transfer mechanism with temperature (ref. 8).



Figurer S6. Representative Arrhenius plots of the LB monolayers of PET-Au nanoparticles. Data were calculated from the respective I-V profiles shown in Figure 1 insets.

Nanoparticle Dropcast Thick Films. In these measurements, a calculated amount of a concentrated solution of the nanoparticles in toluene was dropcast onto the same IDA electrode (totally 25 μg of particles) by using a Hamilton microliter syringe. The films were then examined under an optical microscope to make sure that the entire IDA fingers were buried under the films. The particle films were then dried with a gentle stream of ultra-high purity nitrogen before being introduced into the cryostat for electrochemical measurements. Figure S7 shows the corresponding I-V profiles of the three gold nanoparticles, along with the temperature dependence of the film conductivity (Figure S8). It can be seen that the particle conductivity increases and activation energy decreases with increasing core size. Activation energies for the dropcast films evaluated from the plot (Figure S8) were 93.5 meV (PET-I); 16.8 meV (PET-II), and 10.4 meV (PET-III), which are comparable to those for the LB monolayers, 66.6 meV (PET-I), 20.5 meV (PET-II) and 3.5 meV (PET-III). Note that Murray et al (ref. 3) reported that the activation energy for arenethiolate-capped gold nanoparticle solid films was in the range of 40 to 80 meV, although one should compare the data with caution as the particle core size and dispersity are different in these two studies.

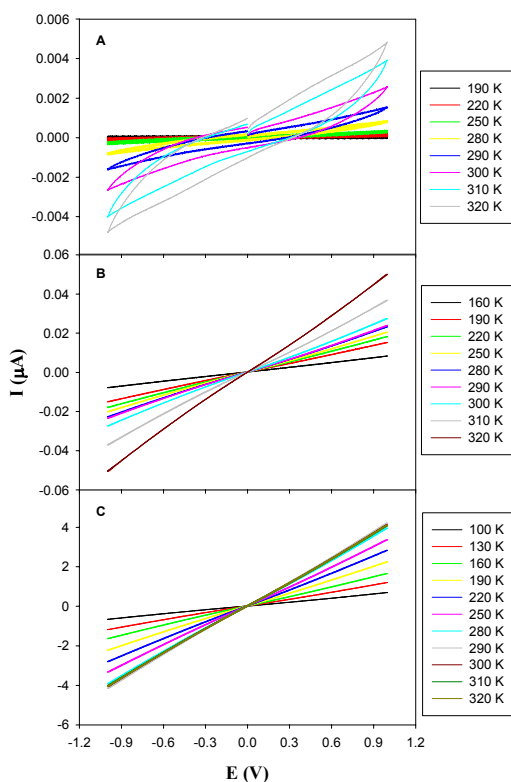


Figure S7. I-V profiles of dropcast thick films of the three PET-Au nanoparticles at varied temperatures: (A) PET-I, (B) PET-II, and (C) PET-III.

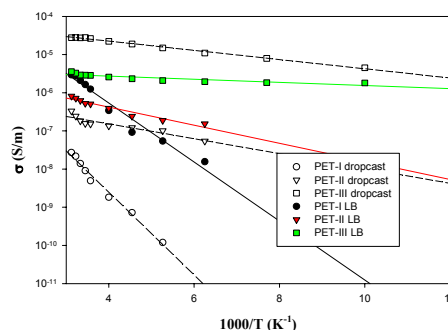


Figure S8. Arrhenius plots of dropcast thick films and LB monolayers (at $l = 1.36$ nm) of PET-Au nanoparticles. Symbols are experimental data calculated from Figure S7 and Figure 1 respectively. Lines are linear regressions.